

Development and Application of Computational Tool Using Local Surface Inclination Methods for Preliminary Analysis of Hypersonic Vehicles

Tiago Cavalcanti Rolim^{1,*}, Sheila Cristina Cintra², Marcela Marques da Cruz Pellegrini³

How to cite

Rolim TC  <https://orcid.org/0000-0002-3711-2044>
Cintra SC  <https://orcid.org/0000-0002-0150-3908>
Pellegrini MMC  <https://orcid.org/0000-0002-8173-1264>

Rolim TC; Cintra SC; Pellegrini MMC (2020) Development and Application of Computational Tool Using Local Surface Inclination Methods for Preliminary Analysis of Hypersonic Vehicles. *J Aerosp Technol Manag*, 12, e2120. <https://doi.org/10.5028/jatm.v12.1123>

ABSTRACT: This work presents a computational tool for preliminary analysis of hypersonic vehicles, based on local surface inclination methods: the HipeX. This program was developed for reading standard triangulation language (STL) geometry files and calculating pressure coefficient and temperature distributions over vehicle's surface using the Newtonian, modified Newtonian or tangent-wedge methods. Validations were made with a cylinder and a sphere, where only the Newtonian method was applied, and with experimental data from Apollo capsule at Mach 10, where the Newtonian and the modified Newtonian methods were applied. These validations presented the code capability to read geometries as well as to estimate aerodynamic force coefficients. A preliminary application was to predict the aerodynamic force coefficients of a generic hypersonic vehicle over constant dynamic pressure trajectories of 23,940, 60,000 and 95,760 N/m² with zero angle of attack. With a fixed dynamic pressure of 60,000 N/m², this vehicle was tested over several Mach numbers and with angle of attack variation from -10 to 10 deg. Zero angle of attack investigation showed minor changes on the force coefficients with altitude, while the variation of angle of attack produced more pronounced variations on these parameters. Maximum flow temperatures over vehicle's surface were estimated ranging from 850 to 5,315 K.

KEYWORDS: Hypersonics; Aerospace vehicles; Aerodynamics; Aerospace systems.

INTRODUCTION

Many experimental researches in flight or at ground facilities have been made to assist the development of hypersonic vehicles. However, given the high costs to perform experimental tests in hypersonic regime, mainly due to the required high enthalpy, new computational tools are needed to simulate tests at this flight regime and provide designers with preliminary data during the conceptual phase. In this sense, early development began with computer programs like the supersonic-hypersonic arbitrary-body program USAF MARK IV (Gentry *et al.* 1973), for evaluation of aerodynamic characteristics of complex shapes. Some characteristics of that tool are the flexibility and the multitude of methods which can be employed.

It is widely known that to take into account all the hypersonic flow effects high computational costs would be required. That is because high-speed flight is associated with high-temperature flow effects, such as excitation of the vibrational mode in diatomic

1. Departamento de Ciência e Tecnologia Aeroespacial - Instituto de Estudos Avançados - Divisão de Aerotermodinâmica e Hipersônica - São José dos Campos/SP - Brazil
2. Universidade Federal de São Paulo - Engenharia de Materiais - São José dos Campos/SP - Brazil
3. Universidade Federal de Itajubá - Engenharia Mecânica Aeronáutica - Itajubá/MG - Brazil

*Corresponding author: tiagotcr@fab.mil.br
Received: 13 Nov 2018 | Accepted: 28 Dec 2019
Section Editor: Alison Moraes



molecules, dissociation and ionization. Also, the very high temperature inside the boundary-layer makes the viscous flow analysis a very important issue (Gulli *et al.* 2012; Pish *et al.* 2019). Indeed, several Navier–Stokes solvers can be found elsewhere such as LAURA (Cheatwood and Gnoffo 1996), the software VULCAN for scramjet applications (White and Morrison 1999), FUN3D (Anderson and Bonhaus 1994) and the ANSYS Fluent (ANSYS 2019). Despite that, rapid estimates for pressure distribution can be obtained using local surface inclination methods (Anderson 1989). So far, the HipeX tool has the capability of using the following methods: Newtonian, modified Newtonian, and tangent-wedge. Newtonian and modified Newtonian methods are most used for blunted body geometries (where normal shockwaves are established) and tangent-wedge method is most used for slender geometries (where plane oblique shockwaves are established).

In this paper, it is discussed how the geometry is imported, it is given a short explanation of the applied methods, how force coefficients are calculated, the allowed strategies for trajectories and software interfaces. Moreover, results from the code validation with simple geometries as well as with Apollo capsule reentry data are shown. Finally, a generic hypersonic vehicle is tested over prescribed trajectories.

METHODOLOGY

The HipeX computer program consists of three interfaces: the geometry interface, a trajectory interface, if the user decides to use it, and an interface for the methods.

GEOMETRY READING

Geometry files in the standard triangulation language (STL) format were chosen for this work due to its simplicity to represent surfaces and because it is widely used on computer-aided design (CAD) tools. In such format, the solid can be represented in two different ways: binary and ASCII. Regardless the choice, the STL file format divides the solid surface into various triangles, storing the positions of the vertices and the components of the normal vectors. Figs. 1 and 2 show the typical configurations of STL file format for ASCII and binary, respectively. All geometries were developed using Autodesk Inventor (Autodesk 2018) as well as the STL files.

```
solid
facet normal ni nj nk
  outer loop
    vertex v1x v1y v1z
    vertex v2x v2y v2z
    vertex v3x v3y v3z
  endloop
endfacet
endsolid
```

Figure 1. ASCII STL format (Chakravorty 2019).

```
UINT8[80] – Header
UINT32 – Number of triangle
foreach triangle
  REAL32[3] – Normal vector
  REAL32[3] – Vertex 1
  REAL32[3] – Vertex 2
  REAL32[3] – Vertex 3
  UINT16 – Attribute byte count
End
```

Figure 2. Binary STL format (Chakravorty 2019).

Regardless the choice, the program is able to separate the coordinates of each vertex of the triangle and the components of the normal vector. After this storage, the program uses this data to calculate the volume, the area of each triangle created in the STL tessellation, total body area, vertex and face quantities.

The volume of the body, enclosed by the surface, is calculated using the divergent theorem. So, it is calculated through the relation:

$$Vol = \frac{1}{3} \oint (X, Y, Z) \cdot \hat{n} dA \quad (1)$$

which is approximated by:

$$Vol = \frac{1}{3} \sum_{i=1}^N (\bar{X}_i, \bar{Y}_i, \bar{Z}_i) \cdot \hat{n} \Delta A_i \quad (2)$$

where N is the total number of triangles and A, B, and C are vertices of the i-th triangle, with:

$$(\bar{X}_i, \bar{Y}_i, \bar{Z}_i) = \left(\frac{X_A + X_B + X_C}{3}, \frac{Y_A + Y_B + Y_C}{3}, \frac{Z_A + Z_B + Z_C}{3} \right) \quad (3)$$

where \hat{n}_i is the vector normal to the surface of the i-th triangle and the area of this triangle is given by:

$$\Delta A_i = \frac{1}{2} |(Y_A - Y_B)(Z_A - Z_C) - (Y_A - Y_C)(Z_A - Z_B), (X_A - X_C)(Z_A - Z_B) - (X_A - X_B)(Z_A - Z_C), (X_A - X_B)(Y_A - Y_C) - (X_A - X_C)(Y_A - Y_B)| \quad (4)$$

From this relation it is also possible to obtain the total surface area through:

$$A = \sum_{i=1}^N \Delta A_i \quad (5)$$

LOCAL SURFACE INCLINATION METHODS

Local surface inclination methods are in general based on simplifications of the flow field. In such methods, there is no need for a detailed calculation of the flow around the vehicle since the local surface inclination is enough to provide the distribution of the pressure coefficient.

Three methods were utilized in this work: Newtonian, modified Newtonian and tangent-wedge (Anderson 1989). Each of them is able to calculate the pressure coefficient of the body surface. The pressure coefficient is related with the freestream pressure P_0 , velocity V_0 , and density ρ_0 as follows:

$$c_p = \frac{p - p_0}{\frac{1}{2} \rho_0 V_0^2} \quad (6)$$

where p is the local pressure.

Basically, these methods depend on the flow deflection angle θ , which can be determined from the vector operation (see also Fig. 3):

$$\phi = \cos^{-1} \left(\frac{\vec{V}_0 \cdot \hat{n}}{V_0} \right) \quad (7)$$

with

$$\theta = \frac{\pi}{2} - \phi \quad (8)$$

Negative flow deflection angles ($\theta < 0$) correspond to regions inside the shadow of the incident flow, where it is assumed that $C_p = 0$.

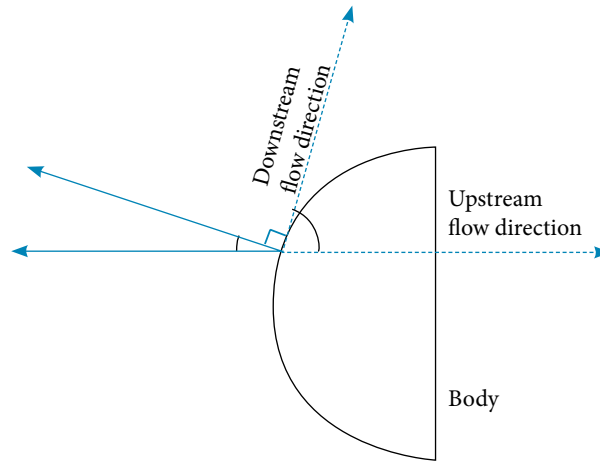


Figure 3. Scheme for calculation of flow deflection angle.

In the Newtonian method, the simplest one, but applicable to two- or three-dimensional bodies in hypersonic regimes, the pressure coefficient is given by:

$$C_{p(Newton)} = 2 \sin^2 \theta \quad (9)$$

The modified Newtonian method is also applicable for two- or three-dimensional bodies in hypersonic flight, but is preferable for blunt-nosed bodies (Anderson 1989). It corrects Newtonian method based on a better estimate of the maximum value of C_p (C_{pMAX}) found at the stagnation point. So, the local pressure coefficient is expressed by:

$$C_p = C_{pMAX} \sin^2 \theta \quad (10)$$

C_{pMAX} is calculated considering that the maximum pressure is achieved when the freestream flow is processed through a normal shock wave and through an isentropic compression, this process corresponds to the Rayleigh pitot tube theory, so that (Anderson 1989):

$$C_{pMAX} = \frac{2}{\gamma_0 M_0^2} \left\{ \left[\frac{(\gamma_0 + 1)^2 M_0^2}{4\gamma_0 M_0^2 - 2(\gamma_0 - 1)} \right] \frac{\gamma_0}{\gamma_0 - 1} \left[\frac{1 - \gamma_0 + 2\gamma_0 M_0^2}{\gamma_0 + 1} \right] \right\} \quad (11)$$

where γ_0 is the ratio of specific heats, assumed to be constant, and M_0 is the flight Mach number.

The accuracy of the Newtonian and modified Newtonian methods tend to improve as the flight Mach number increases as pointed out by Anderson (1989).

The third method which was adopted is the tangent-wedge. It is applicable to slender bodies with two-dimensional shapes on supersonic or hypersonic flow regimes, and obviously extensible for three-dimensional shapes with planar shockwaves. The method assumes that the pressure at the surface can be obtained from a tangent wedge with an equivalent flow deflection angle, by doing such assumption; it is possible to use the oblique shockwave relationships. So, this method is capable of calculating the pressure coefficient as well as other thermodynamic properties (like flow temperature and density).

In fact, it is possible to find the shockwave angle β iteratively from the relation (Anderson 2001):

$$\tan \theta = 2 \frac{M_0^2 \sin^2 \beta - 1}{M_0^2 (\gamma_0 + \cos 2\beta) + 2} \cot \beta \quad (12)$$

Furthermore, the density ratio across the shockwave can be expressed by:

$$p_{ratio} = \frac{(\gamma_0 + 1) M_0^2 \sin^2 \beta}{2 + (\gamma_0 - 1) M_0^2 \sin^2 \beta} \quad (13)$$

The pressure ratio is expressed by:

$$Pratio = 1 + \frac{2\gamma_0}{\gamma_0 + 1} (M_0^2 \sin^2 \beta - 1) \quad (14)$$

And, the temperature ratio is obtained via:

$$Tratio = \frac{Pratio}{p_{ratio}} \quad (15)$$

CALCULATION OF TOTAL FORCE DUE TO PRESSURE

Once C_p is calculated through one of the local surface inclination methods described earlier; the total force due to pressure can be determined by the sum of the contributions of each surface element:

$$\vec{F} = - \frac{\rho_0 V_0^2}{2} \sum_i^N C_{p_i} \hat{n}_i \Delta A_i \quad (16)$$

The force coefficients on the directions X, Y and Z can be found by:

$$\begin{bmatrix} C_x \\ C_y \\ C_z \end{bmatrix} = \frac{\vec{F}}{q_0 S_{ref}} \quad (17)$$

where S_{ref} is the reference area.

Knowledge of coordinate systems is a base point for proper calculation of forces. In particular, the body and wind coordinate systems were used for these simulations (Fig. 4), where it was adopted the same definitions as Zipfel (2007). The body coordinate system is defined by x-axis positive towards the vehicle nose and z-axis is positive down, y-axis is found with the right-hand rule. In the wind coordinate system, the x-axis is defined as parallel and in the direction of the relative wind velocity of the vehicle (with magnitude V_0), the wind z-axis is positive down, the y-axis is obtained from the right-hand rule.

For given angles of attack (α) and sideslip (β), also shown in Fig. 4, the transformation matrix to interchange vectors from the body to the wind coordinate system is:

$$[T]^{WB} = \begin{bmatrix} \cos\alpha \cos\beta & \sin\beta & \sin\alpha \cos\beta \\ -\cos\alpha \sin\beta & \cos\beta & -\sin\alpha \cos\beta \\ -\sin\alpha & 0 & \cos\alpha \end{bmatrix} \quad (18)$$

On the other hand, to transform vectors from the wind to the body coordinate system, one can use:

$$[T]^{BW} = \begin{bmatrix} \cos\alpha \cos\beta & -\cos\alpha \sin\beta & -\sin\alpha \\ \sin\beta & \cos\beta & 0 \\ \sin\alpha \cos\beta & -\sin\alpha \sin\beta & \cos\alpha \end{bmatrix} \quad (19)$$

where, one can see the following properties:

$$[T]^{WB} \cdot [T]^{BW} = \begin{bmatrix} 1 & 0 & 0 \\ 0 & 1 & 0 \\ 0 & 0 & 1 \end{bmatrix} \quad (20)$$

and,

$$[T]^{WB} = [T]^{BW^T} \quad (21)$$

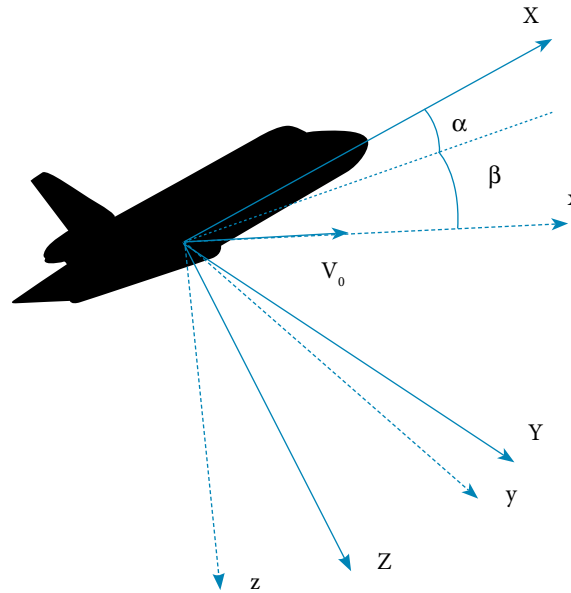


Figure 4. Body (X,Y,Z) and wind (x,y,z) coordinate systems.

Since most of calculations in the code developed is made in the body frame, it is convenient to transform a given flow velocity to the body coordinate system:

$$\vec{V}_0 = \begin{bmatrix} V_x \\ V_y \\ V_z \end{bmatrix} = [T]^{BW} \begin{bmatrix} V_0 \\ 0 \\ 0 \end{bmatrix} \quad (22)$$

Moreover, since the aerodynamic forces are directly related to the forces on the wind coordinate system, one can obtain the drag, lateral force and lift coefficients by applying:

$$\begin{bmatrix} -C_D \\ C_y \\ -C_L \end{bmatrix} = [T]^{WB} \begin{bmatrix} C_x \\ C_y \\ C_z \end{bmatrix} \quad (23)$$

TRAJECTORY STRATEGIES

Three trajectories were chosen for a possible aerospace flight at hypersonic regime: constant dynamic pressure; constant Reynolds number and constant Mach number.

Constant dynamic pressure trajectories work as base for understanding the load limits, very important for the structural design, since all aerodynamic coefficients are proportional to this quantity. The dynamic pressure (q_0) is defined by the atmospheric density and flight velocity on a given altitude as in the equation:

$$q_0 = \frac{\rho_0 V_0^2}{2} \quad (24)$$

The choice of constant Reynolds number can be justified by the fact that laminar or turbulent flow regimes can be inferred by this parameter. In fact, there are many other variables involved in the laminar to turbulent flow transitions; however, as a preliminary estimate, it is a common practice to consider the critical Reynolds number as the sole parameter involved on the transition prediction. Although a precise value of this quantity is generally obtained from experiments, Heiser *et al.* (1994) indicates 10^7 as a good estimate for the beginning of the turbulent flow. The Reynolds number based on freestream properties is defined by:

$$Re_0 = \frac{\rho_0 V_0 L}{\mu_0} \quad (25)$$

where, L is a reference length and μ_0 is the dynamic viscosity of air, calculated using the Sutherland's law (Anderson 1989).

Constant Mach number trajectories are also relevant, and its behavior can be linked to the variations of the atmospheric temperature by means of its dependence on the speed of sound (a_0):

$$M_0 = \frac{V_0}{a_0} \quad (26)$$

Freestream thermodynamic properties were calculated using COESA 1976 atmospheric model (NASA 1976), considering geometric altitude.

SOFTWARE INTERFACES AND FLOWCHARTS

To read the geometry of a solid, the HipeX uses an interface created as seen in Fig. 5. The program starts with the chosen solid, followed by the selection of units. To improve the file compatibility, rotation angles can be supplied by the user so that the solid fits to the coordinate system desired for the simulations. After the reading process, the program uses the acquired data to calculate the volume, the area of each triangle, the total area of the solid's surface, and the numbers of vertices and faces. To check out the importing process, the solid can also be inspected. The flowchart for the reading geometry program is shown in Fig. 6.

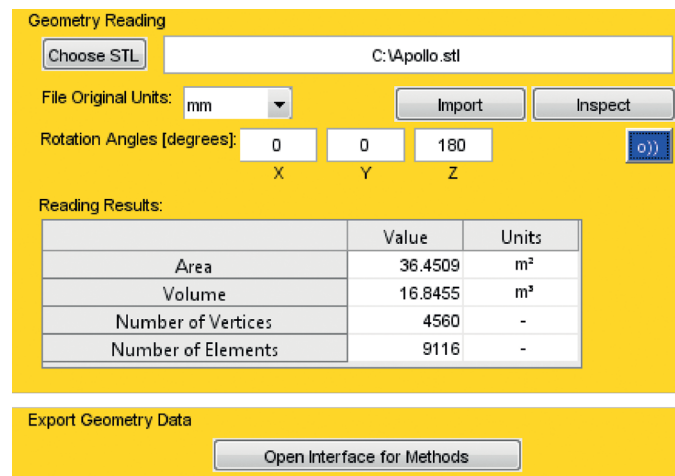


Figure 5. Interface for geometry analysis program.

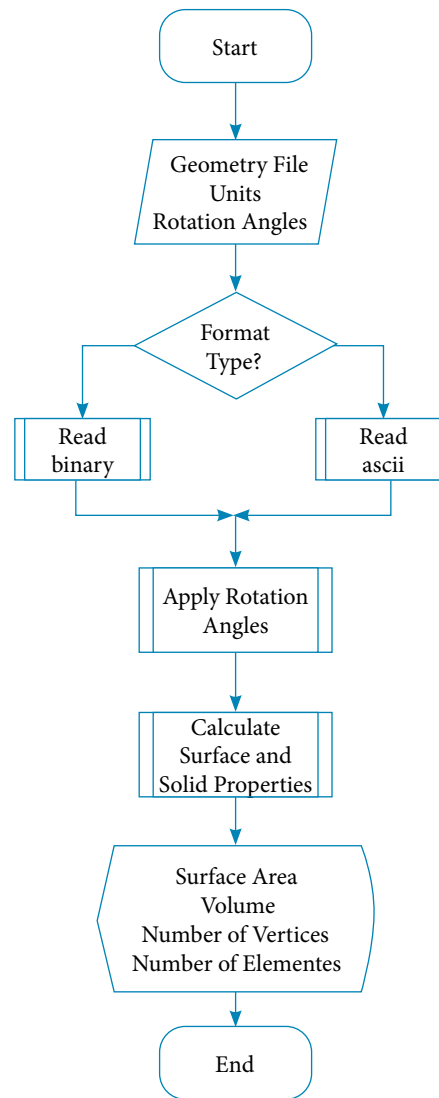


Figure 6. Flowchart for the geometry analysis program.

After reading the geometry, the interface for the methods could be executed. Figure 7 shows the interface for the methods created where the user can choose which method will be used. Also, it is possible to choose if it is a single or a multiple point evaluation. If it is a single point evaluation, the user must provide the flight velocity, angle of attack, and angle of sideslip, reference length and area, and altitude. For a multiple trajectory points, the area and the length must be followed by a trajectory file in XLSX format. If the user decides, the trajectory file can be obtained from the trajectory interface. The flowchart for the surface inclination methods can be seen in Fig. 8.

The interface for trajectory calculations can be seen in Fig. 9, where initial and final altitudes must be provided by the user; the number of discretization points and reference length are also needed as inputs (see Fig. 10 for the flowchart). As stated before, the software gives three possibilities for trajectories: constant dynamic pressure; constant Reynolds number and constant Mach number. The user can choose the most appropriated trajectory and insert the value for the constant. Then, the file is saved in an XLSX file. To check out the calculation, plots can also be made by choosing the most pertinent properties for the user.

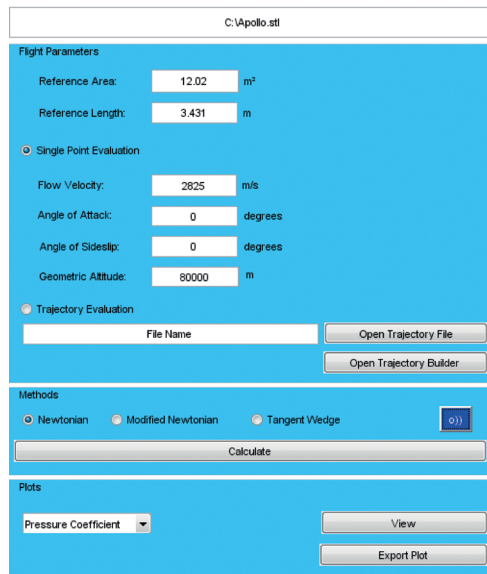


Figure 7. Interface for the program for the surface inclination methods.

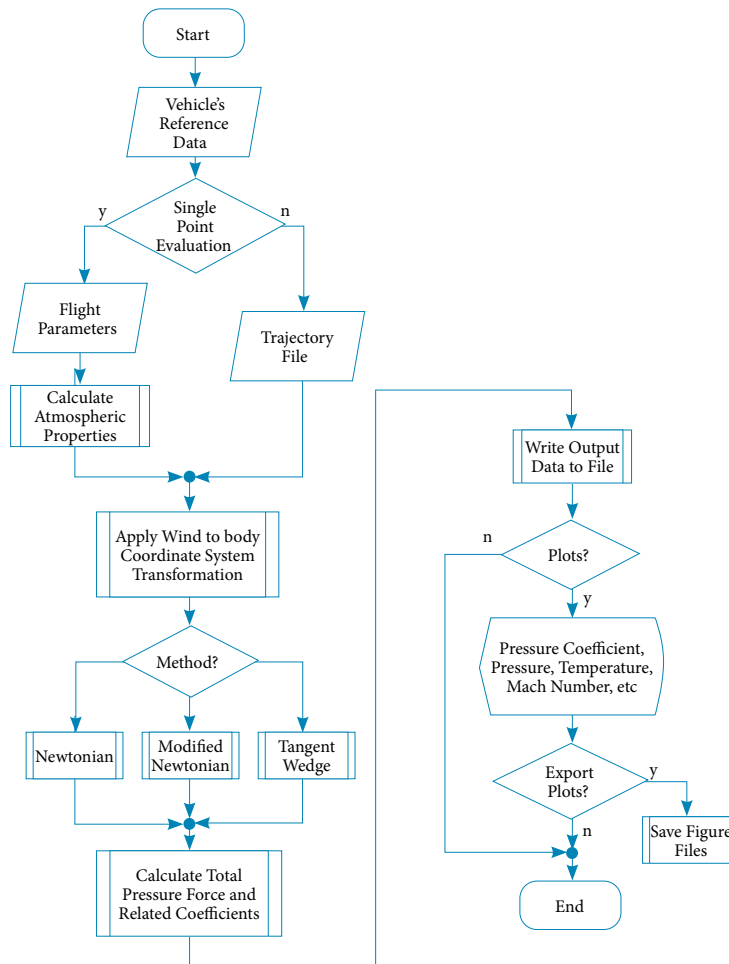


Figure 8. Flowchart for the program for the surface inclination methods.

Parameters

Altitude Variation

Initial Altitude [m]: Number of Points:

Final Altitude [m]:

Strategy

Constant Dynamic Pressure [N/m²] Value of Constant:

Constant Reynolds Number

Constant Mach Number Reference Length [m]:

Results

Horizontal Axis Vertical Axis

Plots

Figure 9. Interface for the trajectory calculation program.

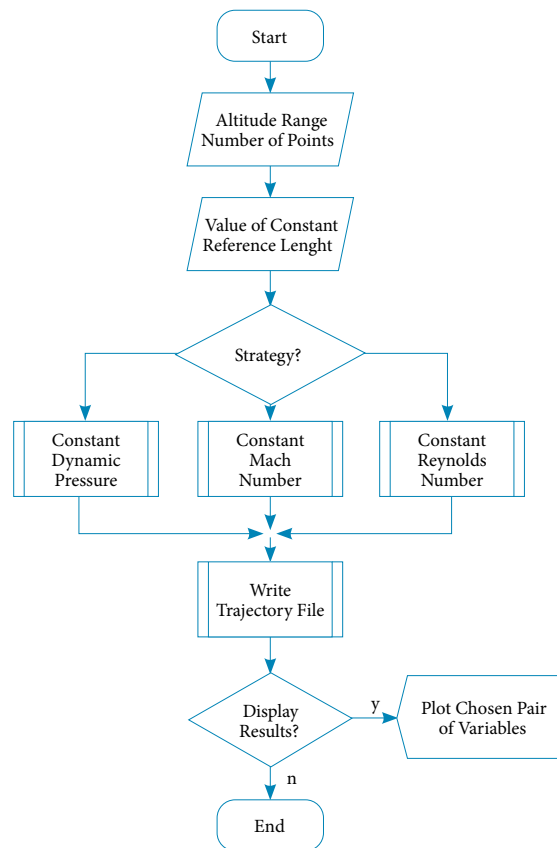


Figure 10. Flowchart for the trajectory calculation program.

RESULTS AND DISCUSSIONS

Parameters for several geometries were evaluated to ensure that the code can be applied in real scenarios. Firstly, elementary geometric bodies with known analytical solutions were used to validate both geometry reading and Newtonian method application processes. Secondly, analysis of Apollo aerodynamic coefficients was conducted to compare the evaluations of HipeX with experimental data. Finally, as application, an arbitrary aerospace vehicle was tested over a prescribed trajectory at zero angle of attack, and also tested for several angles of attack at different Mach numbers.

EVALUATIONS OF SIMPLE GEOMETRIES

It was possible to compare the total area and volume found by the program with the total area and volume from analytical formulas for a cylinder and a sphere (Fig. 11). The results show that the built functions provide values that are very close to the exact values (Tables 1 and 2). The values of the axial force coefficient C_x are compared with the expected values provided by Anderson (1989), only for the Newtonian method. The results are shown in Table 3. The Newtonian method was chosen due to its independence on flight parameters. Again, very good agreement was observed. It is also important to keep in mind that these results depend on the number of vertices and triangles coming from the exporting process used in the CAD. The cylinder was represented by 285 vertices and a total of 566 elements, in binary format, 1.0 m of diameter and 1.0 m high (Fig. 11a). The sphere was composed with 4,514 vertices, with a total of 9,024 elements, in binary format, 1.0 m diameter (Fig. 11b).

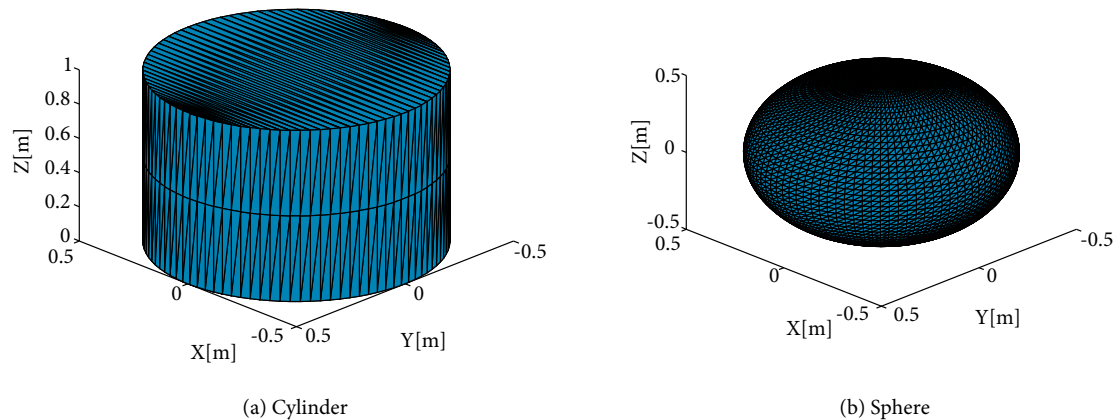


Figure 11. Elementary geometry tests.

Table 1. Comparisons between calculated and analytical values of the surface area.

Geometry	Calculated [m^2]	Theory [m^2]	Deviation
Cylinder	4.7107	4.7124	0.04%
Sphere	3.1388	3.1416	0.09%

Table 2. Comparisons between calculated and analytical values of the volume.

Geometry	Calculated [m^3]	Theory [m^3]	Deviation
Cylinder	0.7848	0.7854	0.08%
Sphere	0.5227	0.5236	0.17%

Table 3. Comparisons between calculated and analytical values for the axial force coefficient C_x , using the Newtonian method.

Geometry	Calculated	Theory	Deviation
Cylinder	-1.3331	-4/3	0.02%
Sphere	-0.9993	-1	0.07%

APOLLO CAPSULE REENTRY

In this study, the purpose was to observe the behavior of the force coefficients in the X and Z directions while the angle of attack was varied from 0 to -30 deg., at Mach 10. The Apollo capsule geometry data was taken from Moss *et al.* (2006) (Fig. 12) and it was represented by 4,560 vertices, 9,116 elements with a reference area of 12.02 m^2 , equivalent to the capsule's maximum cross-section area. A typical run time was less than 200 s for the evaluations over the entire studied range, using an i7-2.20 GHz processor with 8 GB of RAM.

The results are seen in Figs. 13 and 14. The results were compared with those presented by Hirschel and Weiland (2009), where most of the aerodynamic data were obtained from wind tunnel tests. Considering the coefficient of axial force (Fig. 13), the modified Newtonian method presented better results in general. Also, it can be noted that for lower angles of attack the estimate of C_x improves, in fact, the relative deviation when compared to the results of Hirschel and Weiland (2009) is less than 10% when $AOA = 0$ deg. and less than 5% for $AOA = -30$ deg., considering the modified Newtonian method. In the case of the normal force coefficient (Fig. 14), the behavior was different, the modified Newtonian method produced a greater relative deviation for lower values of AOA, for example, at $AOA = -30$ deg. a relative deviation less than 41% was found while the Newtonian method showed a relative deviation of less than 36%. However, the deviations of these two methods decreased notably when the angle of attack approached the null value.

The use of the tangent-wedge method was discarded due to the bow shock expected for the Apollo capsule. This method is more appropriate for attached shockwaves, present on slender geometries.

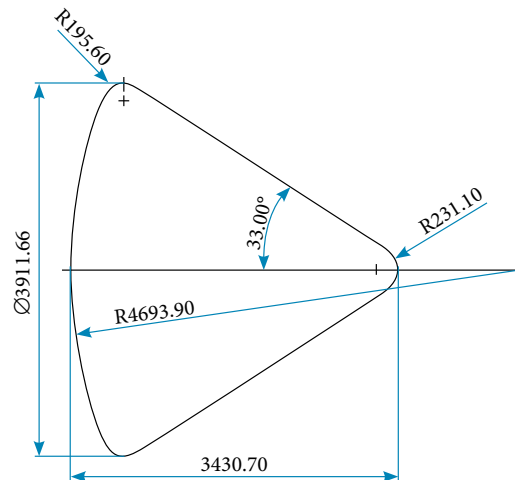


Figure 12. Geometrical data of Apollo capsule (Moss *et al.* 2006).

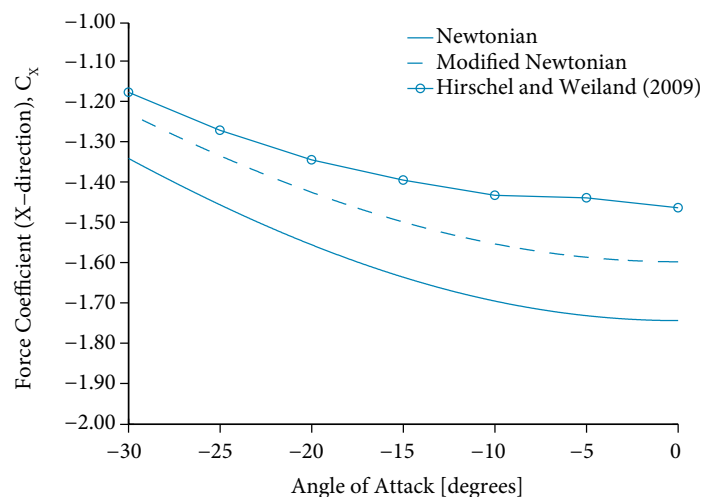


Figure 13. Apollo capsule axial force coefficient (C_x) variation with angle of attack, at Mach 10.

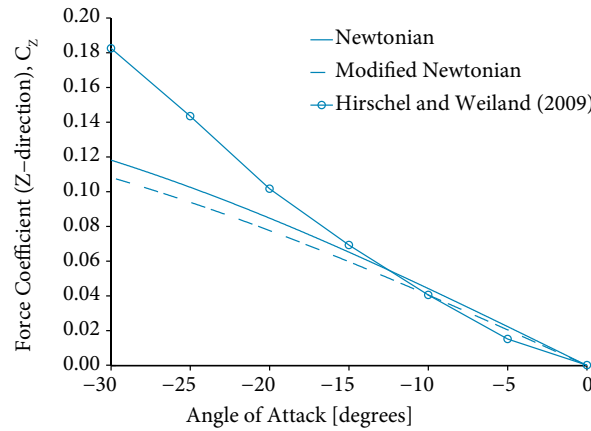


Figure 14. Apollo capsule normal force coefficient (C_z) variation with angle of attack, at Mach 10.

To better assess the code capability, the distribution of C_p according to the Newtonian method for the values of angle of attack 0, -10, -20 and -30 deg. are shown in Fig. 15. For a single point calculation, the run time for this geometry was less than 21 s, including the time for saving results in a spreadsheet file. For the angle of attack 0 deg., the maximum value of $C_p=2$ was reached at the nose center, while in regions located at shadow regions it assumed a null value. When the angle of attack varied, the position of maximum C_p transited away from center.

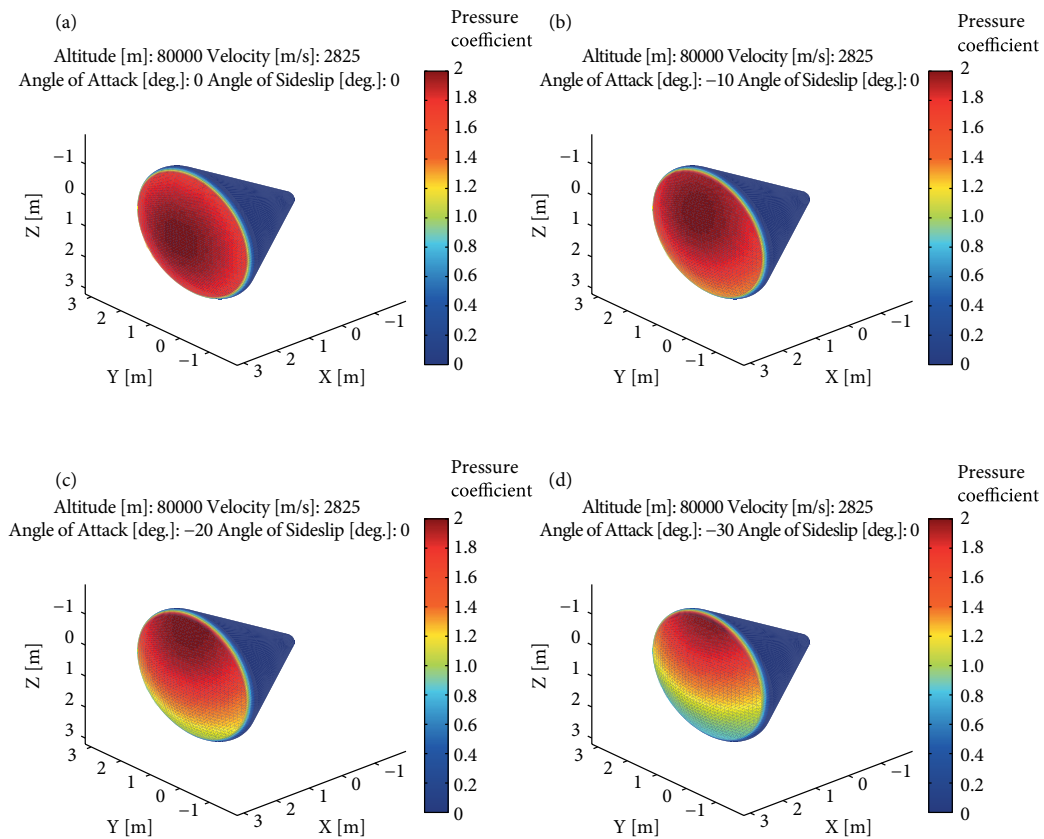


Figure 15. Pressure coefficient distribution over Apollo capsule, Newtonian method at angle of attack: (a) 0 deg.; (b) -10 deg.; (c) -20 deg; (d) -30 deg.

APPLICATION: GENERIC HYPERSONIC VEHICLE

As an application, an aerospace vehicle, shown in Figs. 16 and 17, was designed to test the software capability. The vehicle geometry is formed by a combination of intersecting planes, with sharp edges and faceted surfaces intended to reduce the design and manufacturing costs, with a similar design philosophy presented by Boehrk (2014). The model has 1.0 m of length, 0.894 m of wing span, with a planform area of 0.5 m². The upper ramp has a 10-deg. slope while the lower ramp has a compression angle of 19 deg. The rudder and elevons have symmetric diamond profiles. The STL mesh was composed of 84 elements and 44 vertices.

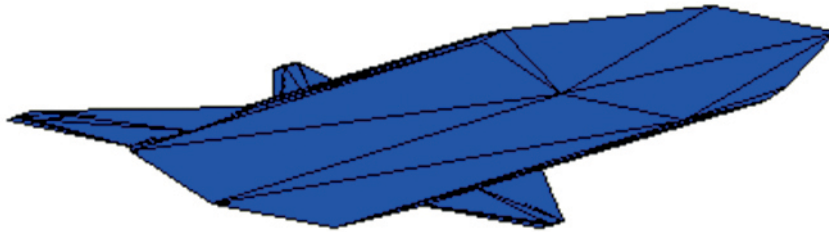


Figure 16. Generic hypersonic vehicle.

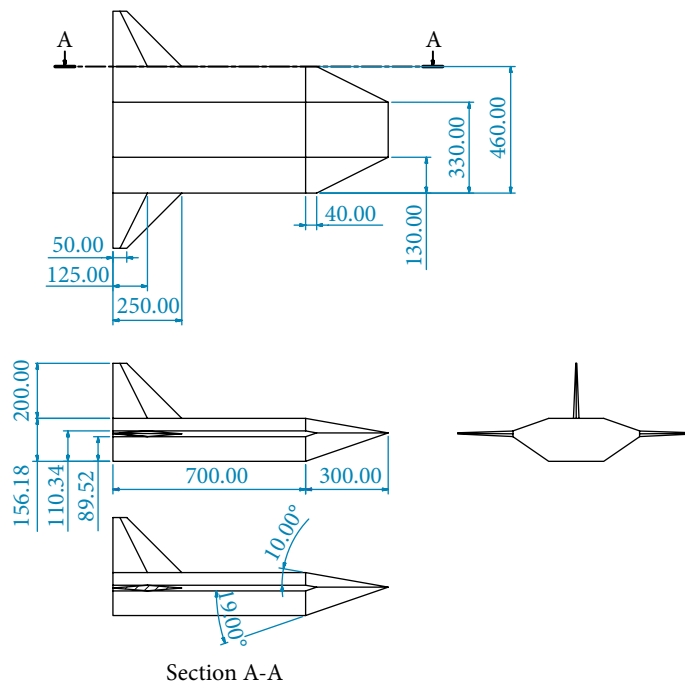


Figure 17. Details of the tested hypersonic vehicle. Dimensions are in mm.

Firstly, flights with constant dynamic pressures of 23,940, 60,000 and 95,760 N/m² with zero angle of attack were simulated. The reasons for these choices were based on the suggested hypersonic airbreathing corridor in terms of dynamic pressure (between 500 and 2,000 lbf/ft²) (Heiser *et al.* 1994), 60,000 N/m² (1,253 lbf/ft²) is an intermediate value. Secondly, the same geometry was tested for various Mach numbers, but keeping a constant dynamic pressure of 60,000 N/m², in which the angle of attack ranged from -10 to 10 deg. The altitude was varied from 30 to 50 km, this altitude range would mimic a typical hypersonic test flight;

the freestream properties were obtained from the trajectory interface. Mach number and velocity varied as depicted in Fig. 18(a) and (b), respectively. The test matrices are shown in Tables 4 and 5. Due to the fact that the chosen geometry only generates attached planar shocks, the most appropriated method was the tangent-wedge, which provided the pressure distribution and consequently the forces applied on the vehicle surface. Moreover, it was possible to obtain the inviscid flow temperature at regions adjacent to the vehicle.

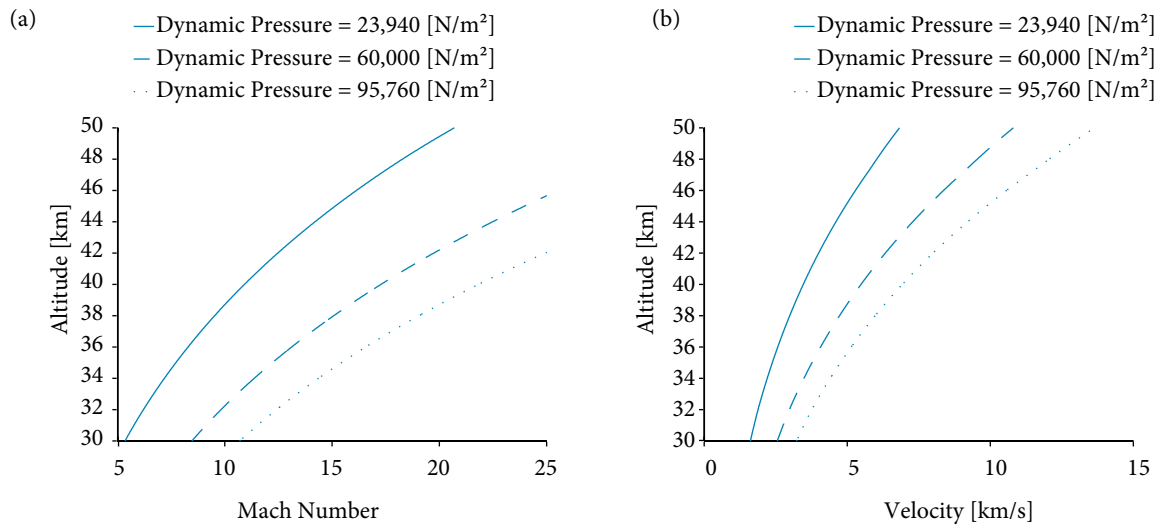


Figure 18. Variation of flight parameters with altitude for constant dynamic pressure trajectories. (a) Mach number; (b) Velocity

Table 4. Test matrix for constant dynamic pressure trajectory studies.

Dynamic pressure [N/m ²]	Altitude [km]	Angle of attack [degrees]
23,940	30–50	0
60,000	30–50	0
95,760	30–50	0

Table 5. Test matrix for angle of attack variation studies.

Dynamic pressure [N/m ²]	Mach number	Angle of attack [degrees]
60,000	9	-10 – +10
60,000	12	-10 – +10
60,000	15	-10 – +10
60,000	25	-10 – +10

For each of the simulated configurations of Tables 4 and 5, the computation time was less than 47 s, with a 1000 points discretization.

The variation of the force coefficient on the X-direction with the altitude can be seen in Fig. 19, the choice of this coefficient was supported by the fact that the drag coefficient is closely related to it. As the altitude varied from 30 to 50 km, the C_x varied from -0.0243 to -0.0192 , for the case of a dynamic pressure of $23,940 \text{ N/m}^2$, this was the greatest variation. The dynamic pressure of $60,000 \text{ N/m}^2$ produced a variation from -0.0213 to -0.0190 while in the case of $95,760 \text{ N/m}^2$ one can see that it varied from -0.0204 to -0.0189 . From one to another dynamic pressure, it can be seen that the difference was more pronounced

at low altitudes, corresponding to lower Mach numbers (Fig. 18a). As the altitude increases, the Mach number increases and the axial force coefficient becomes less sensitive to the Mach number variation. This fact is in accordance with the hypersonic Mach number independence principle, brought by a very thin shock layer, which is a result from the decrease of the shock wave angle with Mach number.

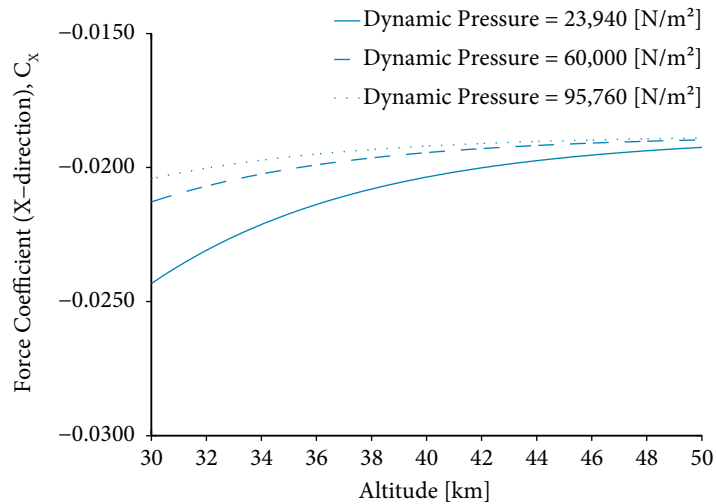


Figure 19. Hypersonic vehicle axial force coefficient (C_x) variation with altitude.

To further investigate the aerospace vehicle behavior, plotted in Fig. 20 are the values of the force coefficient on Z-direction, C_z , for the three cases of dynamic pressures, as the altitude increases. In this parameter, as in the axial force coefficient, lower Mach numbers corresponded to a higher dependence on the altitude and also on the dynamic pressure. For the case of 23,940 N/m², this parameter varied from -0.0346 to -0.0321 . The intermediate case, 60,000 N/m², produced a variation from -0.0328 to -0.0321 . Meanwhile, the highest dynamic pressure of 95,760 N/m² corresponded to a variation from -0.0324 to -0.0320 . Again, as the altitude increases, the normal force coefficient becomes less sensitive to the altitude and dynamic pressure variations.

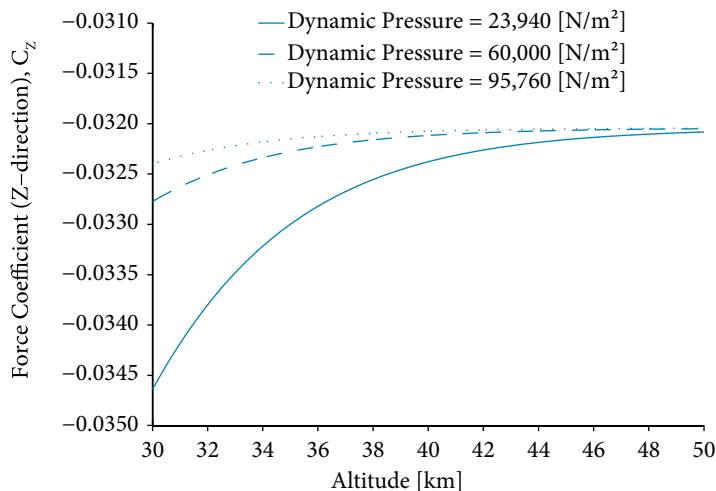


Figure 20. Hypersonic vehicle normal force coefficient (C_z) variation with altitude.

Next, the variation of C_x as the angle of attack changes is shown in Fig. 21 for Mach numbers 9, 12, 15 and 25, all corresponding to a constant dynamic pressure of 60,000 N/m². A large variation of this parameter can be seen as the angle of attack was varied. The largest variation was notable seen for positive angles. As the angle of attack ranged from -10 to +10 deg., the axial force coefficient varied from -0.0163 to -0.0382 in the case of Mach number 9. In a similar fashion, at a higher Mach number of 25, C_x varied from -0.0146 to -0.0367, almost doubled. The curve behavior was slight nonlinear for negative values of angle of attack, meanwhile, for positive values, the variation tended to be more linear. This effect could be explained by the larger angle at the lower surface of the vehicle which causes higher pressures, a 19-deg. ramp, while at the upper surface, the ramp has a 10-deg. inclination, producing mild modifications as the flow is turned negatively.

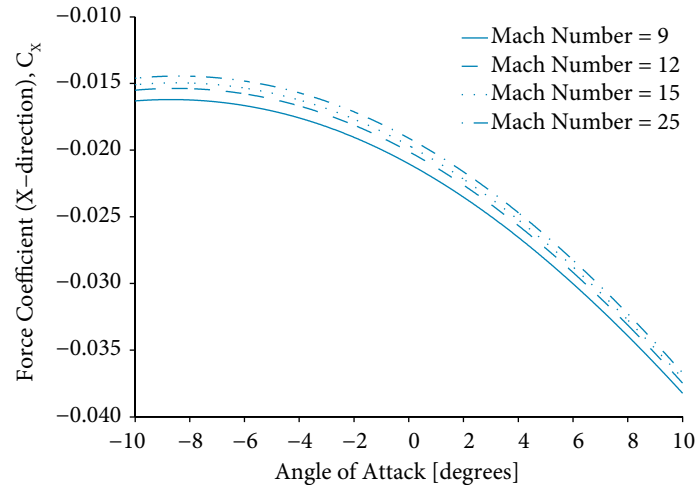


Figure 21. Hypersonic vehicle axial force coefficient (C_x) variation with angle of attack, for several Mach numbers.

Fig. 22 shows the results for C_z as the angle of attack varied. For Mach number 9, C_z varied from 0.1132 to -0.1699. A variation from 0.1014 to -0.1551 was found for the Mach number 25. As can be noticed, the variation of C_z was almost linear for all Mach number cases throughout the studied range of angle of attack and no significant variation was found among the different cases of Mach number, however, minor variations were found near the negative and positive limits of the angle of attack range. On the other hand, it is important to notice that a large variation of C_z was found for positive values of angle of attack, due to the asymmetry of the vehicle.

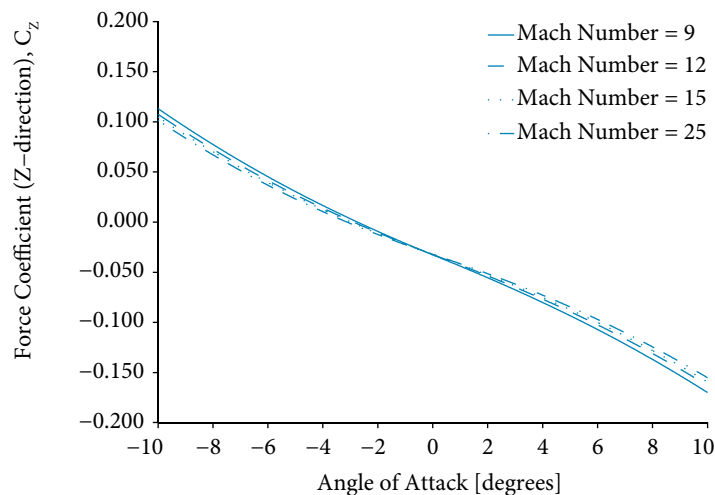


Figure 22. Hypersonic vehicle normal force coefficient (C_z) variation with angle of attack, for several Mach numbers.

Figure 23 shows the contours of pressure coefficient and static temperature on the fluid adjacent to the vehicle surface at Mach numbers of 9 and 25, both on a constant dynamic pressure trajectory of $60,000 \text{ N/m}^2$ with zero angle of attack. In Fig. 23(a), corresponding to the Mach number 9, the maximum value of the pressure coefficient was 0.2763 at the lower compression ramp; this region also was related with the maximum pressure coefficient at Mach 25, as seen in Fig. 23(b), assuming 0.2584 in this case, a decrease of less than 7%. In the regions of shadow, corresponding to zero or negative deflections of the flow with respect to the freestream, C_p is null.

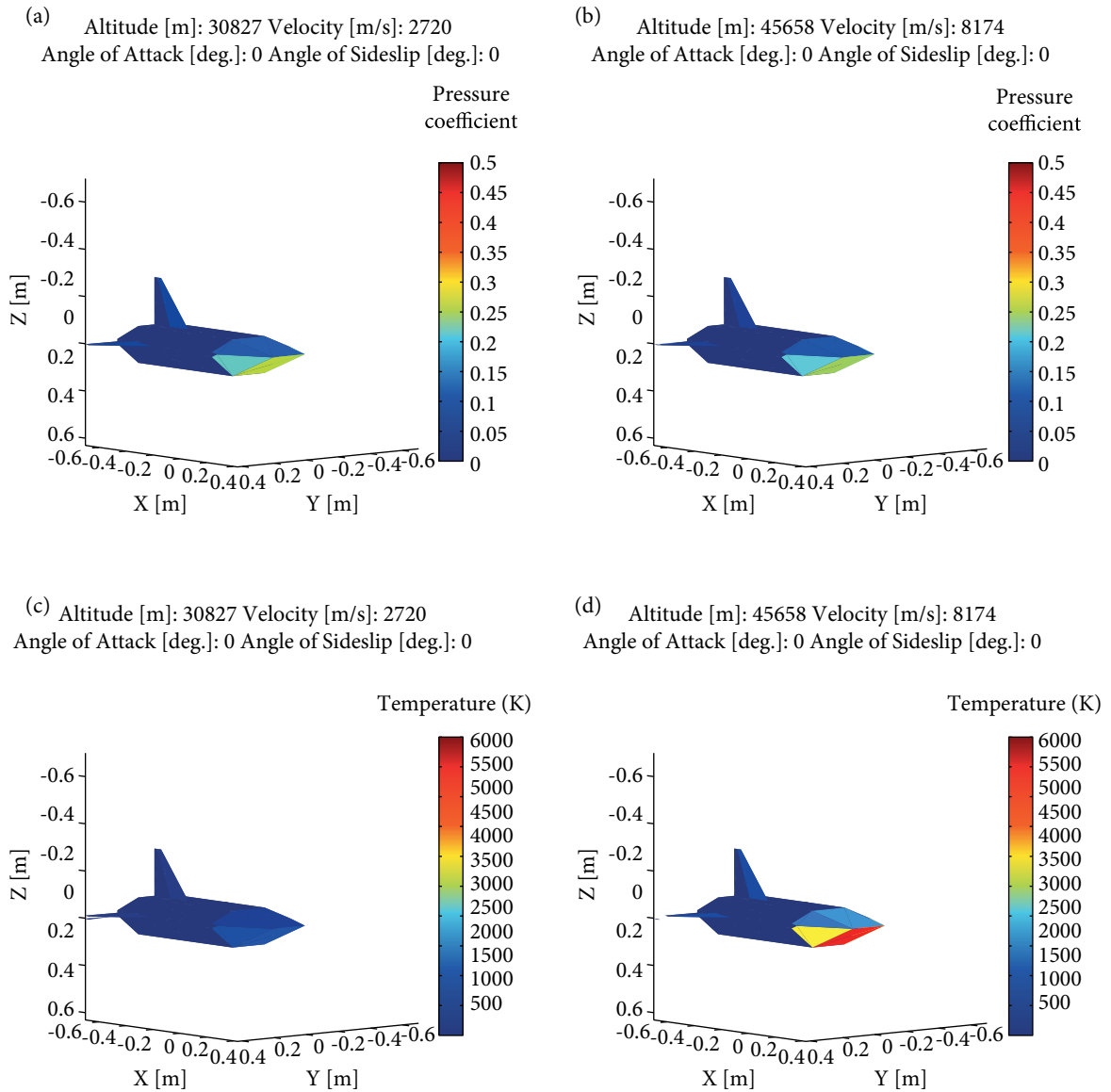


Figure 23. Contour plots of pressure coefficient and temperature distributions for: (a) Mach 9; (b) Mach 25; (c) Mach 9; (d) Mach 25 over the hypersonic vehicle for a constant dynamic pressure of $60,000 \text{ N/m}^2$.

Knowledge of the vehicle's thermal loads is of paramount importance to a preliminary design, so that surface materials, cooling systems, or even reactive heat protection systems would be designed to withstand the high heat transfer rates associated to the hypersonic flight. Temperature estimates were given by Eq. 15. Indeed, Fig. 23(c) shows that flow temperature could be very high, about 850 K, in the case of Mach number 9, while in the case of Mach number 25, the maximum temperature reached on the flow was as high as 5,315 K (Fig. 23d). Moreover, it can be seen that the largest thermal load was in the 19-deg. compression ramp, in both cases. Also, the method predicts that temperatures drop severely when the flow is parallel to freestream flow, corresponding to shadow regions. It is important to notice, however, that it is expected an over prediction of temperatures since no high-temperature effects were taken into account, for instance, excitation of the vibrational mode of the diatomic molecules and dissociation tend to diminish the flow temperature. Also, if boundary layer effects were accounted, considerable changes on the flow temperature around the vehicle could be found.

CONCLUSIONS

The presented work provides a description of the HipeX code, which is an alternative with a relatively low computational cost, based on local surface inclination methods, for aerothermodynamic analysis of hypersonic vehicles. Firstly, it was discussed how the program reads geometry files in STL format, how the surface inclination methods (Newtonian, modified Newtonian and tangent-wedge) are used to obtain the pressure coefficient, how to calculate the total pressure force acting on vehicle's surface, what are the trajectories that could be adopted (constant dynamic pressure, constant Reynolds number or constant Mach number), and the software interfaces.

A validation of the methodology was made on two ways: in the first one, simple geometries with known analytical results for the Newtonian method were considered. Secondly, comparisons were made with experimental data from Apollo capsule and Newtonian and modified Newtonian methods.

As a primary application, a generic hypersonic aircraft was designed and tested over constant pressure trajectories of 23,940, 60,000 and 95,760 N/m² with the tangent-wedge method, firstly with zero angle of attack and secondly with a mild variation of this parameter on selected Mach numbers. The results were focused on the values for the force coefficients. Although during the zero angle of attack investigation the force coefficients showed only minor changes, the angle of attack variation produced considerable variations on these parameters. Moreover, it was possible to investigate how the flow temperature was distributed over the vehicle's surface. Temperatures of the inviscid flow tangential to the vehicle surface were also evaluated. However, high fidelity simulations are indispensable to better predict the thermal state of the surface. Indeed, it should be addressed that the surface temperature is dependent on several parameters not discussed in this work.

Finally, the importance of preliminary tools for aerospace vehicle design relies on the possibility of screening configurations that would best fit the proposed mission, knowledge of advantages or disadvantages can help further development of the selected vehicle configurations. Complex high-fidelity models are of paramount importance to understand the aerodynamics of such vehicles; however, it is possible to estimate many aerodynamic performance parameters with local surface inclination methods with a fraction of the computational cost of a more detailed analysis.

ACKNOWLEDGMENTS

Editors and authors are thankful to Fundação Conrado Wessel for providing the financial support for publishing this article.

FUNDING

Conselho Nacional de Desenvolvimento Científico e Tecnológico.

Grants Nos: 10/ PIBIC-PIBITI/IEAv/2015 and 01/PIBIC-PIBITI/IEAv/201

<http://dx.doi.org/10.13039/501100003593>

AUTHOR'S CONTRIBUTION

Conceptualization, Rolim T. C.; Methodology, Rolim T. C., Cintra S. C. and Pellegrini M. M. C.; Investigation, Rolim T. C., Cintra S. C. and Pellegrini M. M. C.; Writing - Original Draft, Rolim T. C. and Cintra S. C.; Writing - Review and Editing, Rolim T.C.

REFERENCES

- Anderson JD (1989) Hypersonic and High Temperature Gas Dynamics. 2nd ed. London: McGraw-Hill.
- Anderson JD (2001) Fundamentals of Aerodynamics. 3rd ed. London: McGraw-Hill.
- Anderson WK and Bonhaus DL (1994) An implicit upwind algorithm for computing turbulent flows on unstructured grids. *Comput Fluids*. 23(1):1-21. [https://doi.org/10.1016/0045-7930\(94\)90023-X](https://doi.org/10.1016/0045-7930(94)90023-X)
- ANSYS (2019) ANSYS Fluent, Release 19.2, Help System, Fluent Guide. Canonsburg: ANSYS.
- Autodesk (2018) Autodesk Inventor, San Rafael, USA.
- Boehrck H (2014) Transpiration cooling at hypersonic flight – AKTiV on SHEFEX II. In: 11th AIAA/ASME Joint Thermophysics and Heat Transfer Conference. Atlanta: Aviation Forum. <https://doi.org/10.2514/6.2014-2676>
- Chakravorty D (2019) STL file format [3D printing] – Simply explained. ALL3DP. [accessed Apr 15 2020]. <https://all3dp.com/what-is-stl-file-format-extension-3d-printing/#pointone>
- Cheatwood FM, Gnoffo PA (1996) User's manual for the Langley Aerothermodynamic Upwind Relaxation Algorithm (LAURA). Hampton: NASA Langley Research Center. [Accessed Apr 15 2020]
- Gentry AE, Smyth DN, Oliver WR (1973) The Mark IV supersonic-hypersonic arbitrary-body program. Volume II – Program formulation. Ohio: USAF Flight Dynamics Laboratory.
- Gulli S, Maddalena L, Hosder S (2012) Variable transpiration cooling: A new solution for the thermal management of hypersonic vehicles. In: 50th AIAA Aerospace Sciences Meeting including the New Horizons Forum and Aerospace Exposition. Nashville: American Institute of Aeronautics and Astronautics. <https://doi.org/10.2514/6.2012-221>
- Heiser WH, Pratt DT, Daley DH, Mehta UB (1994) Hypersonic airbreathing propulsion. Washington: American Institute of Aeronautics and Astronautics. <https://doi.org/10.2514/4.470356>
- Moss J, Glass C, Greene F (2006) DSMC Simulations of Apollo capsule aerodynamics for hypersonic rarefied conditions. In: 9th AIAA/ASME Joint Thermophysics and Heat Transfer Conference. San Francisco: Meeting Paper. <https://doi.org/10.2514/6.2006-3577>
- NASA (1976) U.S. Standard Atmosphere, 1976. Washington: NASA-TM-X-74335.
- Pish F, Hassanvand A, Gerdoodbary MB, Noori S (2019) Viscous equilibrium analysis of heat transfer on blunted cone at hypersonic flow. *Case Stud Therm Eng*. 14:100464. <https://doi.org/10.1016/j.csite.2019.100464>
- Hirschel E, Weiland C (2009) Selected aerothermodynamic design problems of hypersonic flight vehicles. Heidelberg: Springer-Verlag Berlin. <https://doi.org/10.2514/4.479908>
- White JA, Morrison JH (1999) A pseudo-temporal multi-grid relaxation scheme for solving the parabolized Navier–Stokes equations. In: 14th Computational Fluid Dynamics Conference. Norfolk: Meeting Paper. <https://doi.org/10.2514/6.1999-3360>
- Zipfel PH (2007) Modeling and simulation of aerospace vehicle dynamics. 2nd ed. Reston: American Institute of Aeronautics and Astronautics. <https://doi.org/10.2514/4.862182>